Soft Matter

PAPER

View Article Online
View Journal | View Issue

How ions in solution can change the sign of the critical Casimir potential

Cite this: *Soft Matter*, 2014, **10**, 470

Faezeh Pousaneh,[a] Alina Ciach[a] and Anna Maciołek[bca]

We show that hydrophilic ions present in a confined, near-critical aqueous mixture can lead to an attraction between like charge surfaces with opposing preferential adsorption of the two species of the mixture, even though the corresponding Casimir potential in uncharged systems is repulsive. This prediction agrees with a recent experiment [Nellen *et al.*, *Soft Matter*, 2011, **7**, 5360]. We also show that oppositely charged hydrophobic surfaces can repel each other, although the Casimir potential between uncharged surfaces with like preferential adsorption (selectivity) is attractive. This behavior is expected when the electrostatic screening length is larger than the correlation length, and one of the confining surfaces is strongly selective and weakly charged, whereas the other confining surface is weakly selective and strongly charged. The Casimir potential can change sign because the hydrophilic ions near the weakly hydrophobic surface can overcompensate the effect of hydrophobicity, and this surface can act as a hydrophilic one. We also predict a more attractive interaction between charged, hydrophilic surfaces and a more repulsive interaction between charged, hydrophobic surfaces than given by the sum of the Casimir and Debye–Hückel potentials. Our theory is derived systematically from a microscopic approach, and combines the Landau-type and Debye–Hückel theories with an additional contribution of an entropic origin.

Received 20th July 2013
Accepted 31st October 2013

DOI: 10.1039/c3sm51972d

www.rsc.org/softmatter

I. Introduction

Properties of colloidal systems depend crucially on effective interactions between the colloid particles.[1,2] For this reason the possibility of tuning these interactions by reversible changes of some control parameter is of great interest in colloidal science. Temperature is a thermodynamic parameter that can be easily changed in a reversible manner, therefore temperature controlled thermodynamic Casimir potential draws increasing attention.[3–7] The thermodynamic Casimir forces arise near the critical point of a fluid confined between two surfaces (*e.g.* surfaces of particles) as a result of critical fluctuations and they act between the confining surfaces.[3,4,8–11] The critical temperature is close to room temperature for the demixing transition in mixtures of water and organic liquid (oil) such as lutidine or methylpyridine.[3–5,7,12] The confining surfaces are either hydrophilic or hydrophobic, therefore excess of water or oil appears in near-surface layers of a thickness comparable to the correlation length ξ. When the critical point with the critical temperature T_c is approached, then the correlation length increases, $\xi \propto |\tau|^{-\nu}$, where $\tau = (T - T_c)/T_c$ and $\nu \approx 0.63$.[4,6,13] When the distance between the two surfaces is $L \sim \xi$, then the adsorbed layers overlap and influence each other. The L-dependent modification of the concentration profile leads in turn to the L-dependent excess grand potential, *i.e.* the excess pressure. For $L/\xi \gg 1$ the Casimir potential per unit area between parallel surfaces decays exponentially, $\beta V_C(L) = \frac{A_C}{\xi^2}\exp(-L/\xi)$, with $A_C = -1.51(2)$ and $A_C = 1.82(2)$ for like and opposite adsorption preferences respectively.[4] Thus, surfaces with like adsorption preferences attract each other, whereas opposing adsorption preferences lead to a repulsion.[3,4,10,11,14] Moreover, the potential is independent of the strength of the surface–fluid interaction h_1 that measures the hydrophilicity or hydrophobicity of the surfaces. We note, however, that the temperature range $|\tau|$ corresponding to the above universal behavior shrinks with decreasing h_1.[15,16] In the case of very weakly adsorbing surfaces, the Casimir potential can deviate from the above form for the experimentally accessible range of τ.[14–17] Because of the strong dependence of ξ on temperature, the range of the Casimir potential can be easily changed.

In systems such as the colloidal suspensions, the van der Waals and electrostatic interactions between the colloidal particles are also present. The former can be eliminated by a refractive-index matching. The latter can be screened by adding salt to the solution. The electrostatic potential per unit area between two parallel

[a]*Institute of Physical Chemistry, Polish Academy of Sciences, Kasprzaka 44/52, PL-01-224 Warsaw, Poland*

[b]*Max-Planck-Institut für Intelligente Systeme, Heisenbergstraße 3, D-70569 Stuttgart, Germany*

[c]*IV. Institut für Theoretische Physik, Universität Stuttgart, Pfaffenwaldring 57, D-70569 Stuttgart, Germany*

charged surfaces immersed in electrolyte decays exponentially for large separations, $\beta V_{el}(L) \simeq \frac{2\kappa\sigma_0\sigma_L}{\bar{\rho}_{\mathrm{ion}}} \exp(-\kappa L)$, where $e\sigma_0$ and $e\sigma_L$ are surface charges, e is the elementary charge, κ is the inverse Debye screening length and $\bar{\rho}_{\mathrm{ion}}$ is the number density of ions.[13,18]

The sum of the Casimir and electrostatic potentials has the form

$$\beta V(L) = \frac{A_{\mathrm{C}}}{\xi^2} \exp(-L/\xi) + \frac{2\kappa\sigma_0\sigma_L}{\bar{\rho}_{\mathrm{ion}}} \exp(-\kappa L). \quad (1)$$

The first term in (1) is attractive for like adsorption preferences and repulsive for opposite adsorption preferences. The second term is repulsive or attractive for like or opposite surface charges respectively. Thus, various shapes of $V(L)$ can be obtained for different combinations of the surface properties and for different ratios of the decay rates

$$y = \xi\kappa. \quad (2)$$

The potential can be repulsive or attractive for like signs of the two terms in (1), and a minimum or a maximum for $L \sim \xi$ can appear for opposite signs. The shape of the potential between identical surfaces with large surface charge and $y > 1$ (strong short-range repulsion and weaker long-range attraction) is very similar to the Lennard-Jones potential. The minimum, however, occurs at the separation $L \sim$ 10–100 nm sufficiently close to the critical point and for large screening length. For surfaces with an area typical for colloid particles, the depth of the minimum can be as large as a few $k_{\mathrm{B}}T$, which is enough for inducing phase transitions into the phases rich and poor in the colloid particles.[7] If $V(L)$ has a maximum ($y < 1$ and the surfaces are weakly charged), the resulting short-range attraction long-range repulsion (SALR) effective potential can lead to the formation of dynamic spherical or elongated clusters, a network or layers of particles, as observed in the case of depletion attraction instead of the Casimir potential.[19–24] By varying the temperature and thereby changing the bulk correlation length ξ, one can cause the attractive well or the repulsive barrier in the effective potential to appear and to disappear. Thus, it seems possible to induce or to suppress a macro- or microphase separation by small temperature changes. Indeed, analogs of the gas, liquid and crystal phases were induced and destroyed by temperature changes within $0.5C$.[7]

Experimental results show, however, that the effective potential can strongly deviate from the sum of the Casimir and the electrostatic potentials, even when no other interactions are present. The experimental results obtained in ref. 4 for $y > 1$ could not be fitted with eqn (1). Only for distances much larger than the position of the potential minimum it was possible to fit the universal Casimir potential with the experimental results, because for $y > 1$ and $\kappa L \gg 1$ the electrostatic contribution is negligible. In another experiment[6] an attraction was measured between like charge hydrophilic and hydrophobic surfaces for some temperature range corresponding to $y < 1$. Both the electrostatic and the Casimir potentials are repulsive, and according to eqn (1) should lead together to enhanced repulsion. The experimental result of ref. 6 is in complete disagreement with eqn (1). The above strong quantitative[4] and even qualitative[6] disagreement between eqn (1) and the experiment shows that in order to design effective interactions it is necessary to develop a more accurate theory. Several attempts have been made already.[25–31]

In ref. 28 and 31 the phenomenological Landau-type functional was postulated by adding the Landau functional for the critical solvent and the free energy of the ions. In addition, terms describing the coupling of the density of the anions and the cations with the solvent composition were included. The unusual attraction between like charge hydrophilic and hydrophobic surfaces was obtained in these theories as a result of different solubilities of the anion and the cation in water, and different interactions of the two ionic species with the surfaces.

In this work we further develop the theory introduced and studied in ref. 25–27, where the Landau-type approach was derived from a microscopic lattice gas model for a four component mixture, and also from a simple density functional theory (DFT). We took into account van der Waals (vdW) type of interactions between all the components in addition to the Coulomb interactions between the ions. We have assumed the vdW interactions consistent with much bigger solubility of the ions in water than in oil, and neglected the difference in solubilities of the anion and the cation in water. A similar assumption was made for the interactions with the surfaces. After a systematic coarse-graining procedure appropriate in the critical region, a Landau-type functional containing also the electrostatic energy contribution was obtained.

In our theory the dominant contribution to the effective interaction between the surfaces is similar to eqn (1). However, because of the mutual influence of the solvent composition and the charge distribution, the prefactors in (1) should be replaced by the amplitudes that both depend on the surface charges, the fluid–wall interactions and on the ratio of the decay lengths y. For $y > 1$, corresponding to the experiment in ref. 3, a satisfactory quantitative agreement was obtained for 4 different combinations of surfaces in ref. 27. For $y < 1$ we have obtained only preliminary results presented in ref. 26. We considered only like-charge hydrophilic and hydrophobic surfaces, and obtained qualitative agreement with the experimental studies.[6] Different solubilities of the anion and the cation in water neglected in our theory and taken into account in ref. 28 and 31 probably play some role in experiments.[6] Since only our theory agrees quantitatively with the experiment,[4] we believe that it captures the key physical phenomena of the confined near-critical mixture containing ions with preferential solubility in one of the solvent components.

In this article a systematic and complete analysis of all possible combination of selectivity and surface charges of the two confining surfaces is presented within the theory developed in ref. 25–27. The theory is further simplified, and in the new version the essential physics is amplified. Our presentation is organized as follows. We introduce the new version of the theory in Section II. In particular, the order parameter (OP) suitable for the phase separation into a phase rich in water and ions, and a phase rich in lutidine and poor in ions is defined. In Section III we derive and analyze approximate analytical

expressions for $y < 1$. In particular, we show that oppositely charged surfaces with similar adsorption preferences can repel each other for some range of y even though both terms in (1) are attractive. Comparison with numerical results is shown in Section V for a few representative cases. Section VI contains summary and discussion.

II. The generic model

We consider a mixture of water and organic liquid containing a small amount of hydrophilic ions. The mixture is confined between two parallel walls separated by the distance $L \gg a$, where a^3 is the average volume per particle in the liquid phase. The walls are chemically homogeneous, selective and charged with area $A \gg L^2$, and we assume $A \to \infty$ (see Fig. 1).

The fluid between the surfaces is also in contact with a reservoir with fixed temperature and chemical potential of all the components. In equilibrium the distribution of the components in the slit corresponds to the minimum of the grand potential

$$\Omega = A\omega = A\left[u_{\mathrm{vdW}} + u_{el} - Ts - \int_0^L \mathrm{d}z\mu_i\rho_i(z)\right], \qquad (3)$$

where $S = As$ denotes entropy, $\rho_i(z)$ and μ_i are the local number density and the chemical potential of the i-th component, respectively, with $i = w, l$ (1,2) corresponding to water and organic solvent (lutidine here), and $i = +, -$ (3,4) corresponding to the cation and the anion. Summation convention for repeated indices is assumed. Due to the charge neutrality $\mu_+ = \mu_-$. We consider dimensionless distance and dimensionless ρ_i, *i.e.* length is measured in units of a, and $\rho_i = a^3N_i/V$, where N_i denotes the number of the i-th kind particles in the volume V. We neglect compressibility of the liquid and assume that the total density is fixed,

$$\sum_{i=1}^{4}\rho_i = 1. \qquad (4)$$

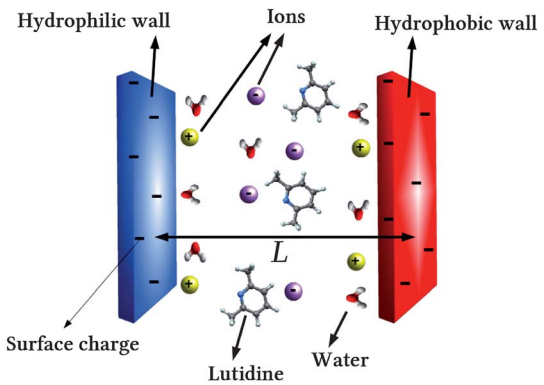

Fig. 1 Schematic representation of the system consisting of water, organic liquid (for example lutidine) and ions between selective and charged parallel walls separated by the distance L much larger than the size of the molecules.

The microscopic details, in particular different sizes of molecules, are disregarded, since we are interested in the density profiles on the length scale much larger than a.

The electrostatic energy per surface area is given by[13,25,27]

$$u_{el} = \int_0^L \mathrm{d}z\left[-\frac{\varepsilon}{8\pi}(\nabla\psi)^2 + e\rho_{\mathrm{q}}\psi\right] + e\sigma_0\psi(0) + e\sigma_L\psi(L), \qquad (5)$$

where ψ is the electrostatic potential which satisfies the Poisson equation

$$\nabla^2\psi(z) = -\frac{4\pi e}{\varepsilon}\rho_{\mathrm{q}}(z), \qquad (6)$$

with the Neumann boundary conditions (BC),

$$\nabla\psi(z)|_{z=0} = -\frac{4\pi e}{\varepsilon}\sigma_0, \quad \nabla\psi(z)|_{z=L} = \frac{4\pi e}{\varepsilon}\sigma_L, \qquad (7)$$

appropriate in the case of fixed surface charges. In the above ε is the dielectric constant, $e\sigma_0$ and $e\sigma_L$ are the surface charges at the two walls, and

$$e\rho_{\mathrm{q}}(z) = e(\rho_+(z) - \rho_-(z)) \qquad (8)$$

is the charge density.

Finally, $U_{\mathrm{vdw}} = Au_{\mathrm{vdw}}$ is the contribution to the internal energy associated with the vdW interactions between all the components. Because of the universality of critical phenomena, the detailed form of the interactions is irrelevant. The density profiles at the length scale $\xi \gg a$ can be obtained from highly simplified models, such as the lattice gas model of a mixture, where only nearest-neighbors interact with the coupling constant J_{ij} between the i-th and j-th components. In continuous models the relevant energy parameter is $J_{ij} = \frac{1}{2d}\int d\mathbf{r}V_{ij}(r)$, where $V_{ij}(r)$ is the interaction potential between the i-th and j-th components, and d is the space dimension. The solubility of inorganic ions in water is much higher than in organic solvents. We can expect that the vdW interaction between the cation and a given species is similar to the vdW interaction between the anion and this species. In ref. 25–27 it was assumed that $J_{+i} = J_{-i}$. Here we make further simplifying assumptions. The mixture separates into a phase rich in water and ions, and a phase rich in lutidine and poor in ions. From the point of view of the phase separation water and ions play a similar role, and the vdW interactions between water and a given species should be comparable to the vdW interactions between the ion and this species. We thus make additional assumption, $J_{wi} = J_{+i} = J_{-i}$. In the critical region we can perform the coarse-graining procedure as described in ref. 25, and after some algebra obtain the vdW contribution to the internal energy (up to a constant) of the form

$$u_{\mathrm{vdW}}/J = \int_0^L\left[-\mathrm{d}\Phi^2 + \frac{1}{2}(\nabla\Phi)^2\right]\mathrm{d}z + \frac{1}{2}\left(\Phi(0)^2 + \Phi(L)^2\right) - h_0\Phi(0) - h_L\Phi(L), \qquad (9)$$

where

$$\Phi(z) = \rho_w(z) + \rho_{\mathrm{ion}}(z) - \rho_l(z) \qquad (10)$$

is the critical order parameter, and

$$\rho_{\mathrm{ion}}(z) = \rho_{+}(z) + \rho_{-}(z) \tag{11}$$

is the number density of ions, h_0 and h_L are the interactions with the surfaces in J-units, and $J = \frac{1}{4}(J_{ww} + J_{ll} - 2J_{wl})$ is the single energy parameter relevant for the phase separation. Note that since in the phase separation water and ions play similar roles (both prefer the same phase), Φ is the natural OP for this phase transition. In the absence of ions Φ reduces to the order parameter of the symmetrical binary mixture, $\rho_w - \rho_l$, and vanishes at the critical demixing point. Real mixtures are not symmetrical, and the OP (10) should be replaced by $\Phi(z) - \bar{\Phi}$, where $\bar{\Phi}$ is the bulk critical value. However, the effective potential between confining surfaces depends on the deviations of the composition from its critical value and not on this value itself. For this reason the symmetrical mixture or the lattice gas model is commonly used in studies of critical phenomena. We make the same assumption here, and in our symmetrical mixture $\Phi = 0$ at the critical point of the phase separation. Note that eqn (9) could be postulated in a phenomenological approach, since the relevant energy associated with the continuous phase transition is the decrease of the internal energy per unit volume when the mixture becomes phase separated, $-dJ\Phi^2$, where Φ is the proper critical OP. Consistent with the assumption of the symmetrical mixture we postulate the lattice gas or ideal-mixing form for the entropy,

$$-Ts = k_{\mathrm{B}}T\int_0^L \mathrm{d}z \sum_{i=1}^{4} \rho_i(z) \ln\, \rho_i(z). \tag{12}$$

When the total density is fixed (see (4)), there are three independent variables, and the natural choice is ρ_{q}, Φ and ρ_{ion} (see (8), (10) and (11)). We thus consider the grand potential (3) as a functional of these three fields, $\omega[\Phi, \rho_{\mathrm{q}}, \rho_{\mathrm{ion}}]$. In the bulk $\rho_{\mathrm{q}} = 0$ due to the charge neutrality. We limit ourselves to the critical composition, and assume that in the bulk $\Phi = 0$. The bulk density of ions, $\bar{\rho}_{\mathrm{ion}}$, is determined by T and the chemical potential from the condition $\frac{\partial\omega[0,\,0,\,\rho_{\mathrm{ion}}]}{\partial\rho_{\mathrm{ion}}} = 0$, and can be chosen as the independent variable. From the minimum condition of $\omega[\Phi, \rho_{\mathrm{q}}, \rho_{\mathrm{ion}}]$ with respect to $\rho_{\mathrm{ion}}(z)$ we can obtain $\rho_{\mathrm{ion}}(z)$ in terms of $\Phi(z)$ and $\rho_{\mathrm{q}}(z)$ (see Appendix A), and ω becomes a functional of two fields, $\Phi(z)$ and $\rho_{\mathrm{q}}(z)$.

In order to calculate the effective interaction between the surfaces, we have to calculate the excess grand potential per surface area, and subtract the L-independent surface energies (surface tensions) at the two walls. We introduce the functional

$$\mathscr{S}[\Phi, \rho_{\mathrm{q}}] = \omega[\Phi, \rho_{\mathrm{q}}, \rho_{\mathrm{ion}}] - \omega[0, 0, \bar{\rho}_{\mathrm{ion}}], \tag{13}$$

where ρ_{ion} should be expressed in terms of Φ and ρ_{q} as discussed above. $\mathscr{S}$ is the sum of the effective interactions between the surfaces, $\Psi(L)$, and the L-independent surface energies. In the critical region (not too close to the surface) the fields are small, and the entropy (eqn (12)) can be Taylor expanded in terms of Φ and ρ_{q}. In the one-phase region the fourth order terms in the fields can be neglected, and we finally obtain the approximation (see Appendix A)

$$\beta\mathscr{S}[\Phi, \rho_{\mathrm{q}}] \approx \int_0^L \mathrm{d}z \left[\frac{\bar{\beta}}{2}\left(\xi^{-2}\Phi^2 + (\nabla\Phi)^2\right) - \frac{{\rho_{\mathrm{q}}}^2\Phi}{2\bar{\rho}_{\mathrm{ion}}}\right] + \beta\mathscr{S}_{\mathrm{C}}^{\mathrm{s}} + \beta\mathscr{S}_{\mathrm{DH}}[\rho_{\mathrm{q}}], \tag{14}$$

where $\bar{T} = 1/\bar{\beta} = k_{\mathrm{B}}T/J$ is the dimensionless temperature, in the mean-field approximation (MF) the critical temperature is $\bar{T}_{\mathrm{c}} = 2d$ and the bulk correlation length in a-units is $\xi = (\bar{T} - \bar{T}_{\mathrm{c}})^{-1/2}$,

$$\beta\mathscr{S}_{\mathrm{C}}^{\mathrm{s}} = \bar{\beta}\left[\frac{1}{2}\left(\Phi^2(0) + \Phi^2(L)\right) - h_0\Phi(0) - h_L\Phi(L)\right] \tag{15}$$

is the contribution associated with the surfaces, and

$$\beta\mathscr{S}_{\mathrm{DH}}[\rho_{\mathrm{q}}] = \int_0^L \mathrm{d}z \left[\frac{1}{2\bar{\rho}_{\mathrm{ion}}}{\rho_{\mathrm{q}}}^2 + \beta e\rho_{\mathrm{q}}\psi - \frac{\beta\varepsilon}{8\pi}(\nabla\psi)^2\right] + \beta\left(e\sigma_0\psi(0) + e\sigma_L\psi(L)\right). \tag{16}$$

The electrostatic potential ψ satisfies the Poisson equation (6) with the BC (7); for this reason $\beta\mathscr{S}$ is a functional of only two independent fields.

Note that $\frac{{\rho_{\mathrm{q}}}^2(z)}{2\bar{\rho}_{\mathrm{ion}}}$ in eqn (14) plays a role of a position-dependent external field acting on the OP Φ. The physical origin of this "external field" is the excess number density of ions near the charged wall (it decays as ${\rho_{\mathrm{q}}}^2(z)$), and the preferential solubility of the ions in the phase with $\Phi > 0$.

Given the complexity of the considered system, the functional (14) has a rather simple form. At the same time it captures the essential physics of the near-critical mixture containing ions with preferential solubility in one of the mixture components. We believe that this functional can serve as a generic model of such systems. Very close to the critical point it is necessary to add terms $\propto\Phi^4, \Phi^2{\rho_{\mathrm{q}}}^2$ to the integrand in eqn (14), because $\xi^{-1} \to 0$ for $T \to T_{\mathrm{c}}$. This will be a subject of a separate study.

In equilibrium Φ and ρ_{q} take the forms corresponding to the minimum of the functional (14). From $\frac{\delta\mathscr{S}}{\delta\Phi} = 0$ we obtain the first Euler–Lagrange (EL) equation

$$\frac{\mathrm{d}^2\Phi(z)}{\mathrm{d}z^2} = \xi^{-2}\Phi(z) - \frac{\bar{T}{\rho_{\mathrm{q}}}^2(z)}{2\bar{\rho}_{\mathrm{ion}}}, \tag{17}$$

with the boundary conditions (see ref. 25 and 26, but note the difference in the definitions of the surface fields)

$$\Phi'(0) - \Phi(0) = -h_0,\ \Phi'(L) + \Phi(L) = h_L, \tag{18}$$

and from $\frac{\delta\mathscr{S}}{\delta\rho_{\mathrm{q}}} = 0$ we obtain the second EL equation

$$e\psi(z) = -\frac{k_{\mathrm{B}}T}{\bar{\rho}_{\mathrm{ion}}}\rho_{\mathrm{q}}(z)\left(1 - \Phi(z)\right). \tag{19}$$

In the more general case, *i.e.* without the assumption that the difference between the vdW interactions of water and ions is negligible,[27] there are two differential EL equations instead of eqn (17); one for the excess number density of ions and the

other one for the excess solvent concentration. The present analysis is much simpler.

The nonlinear eqn (17) and (19) can be solved numerically. However, when the term $\propto \rho_q{}^2\Phi$ in (14) is treated as a perturbation, we can obtain analytical results in the perturbation expansion, as we did in ref. 27 for $y \gg 1$. In the next section we present the approximate analytical results for the shape of the OP profile and for the excess grand potential in the case of $y < 1$, and compare them with the numerical solutions of the full EL equations.

III. Approximate solutions of the Euler–Lagrange equations

Let us first consider the linearized EL equations,

$$\frac{d^2\Phi^{(1)}(z)}{dz^2} = \xi^{-2}\Phi^{(1)}(z), \tag{20}$$

and

$$e\psi^{(1)}(z) = -\frac{k_B T}{\bar{\rho}_{ion}}\rho_q^{(1)}(z). \tag{21}$$

The Poisson equation and eqn (21) give

$$\frac{d^2}{dz^2}\rho_q^{(1)}(z) = \kappa^2\rho_q^{(1)}(z), \tag{22}$$

with

$$\kappa = \sqrt{\frac{4\pi e^2\bar{\rho}_{ion}}{k_B T\varepsilon}}. \tag{23}$$

In ref. 27 the second term in eqn (17) was neglected, and Φ was approximated by $\Phi^{(1)}$. Thus, only the effect of the critical adsorption on the charge distribution was taken into account for $y > 1$.

As shown in the case of weak surface fields in ion-free systems, the shape of the OP profile can have a strong effect on the Casimir potential.[15,17] It is thus important to determine how the near-surface composition $\Phi(z)$ is influenced by the charge distribution $\rho_q(z)$, and next how the modified shape of $\Phi(z)$ influences the Casimir potential. In this section we focus on this question for $y < 1$. We should note that for $y < 1$ the bulk correlation length is shorter than the screening length, and the system may be at the crossover between MF and the universal critical regime. In this work we shall limit ourselves to the MF approximation. Preliminary results for surfaces with opposite adsorption preferences are presented in ref. 26.

We assume that the surface fields and the surface charge-densities are small and of the same order of magnitude. Thus, the values of ρ_q and Φ are small and comparable, and we can assume that $\Phi - \Phi^{(1)}$, $\rho_q - \rho_q^{(1)} = O(\rho_q^{(1)2}, \Phi^{(1)2})$. In such a case $\rho_q{}^2\Phi$ in (14) can be treated as a perturbation, and eqn (17) and (19) can be approximated by

$$\frac{d^2\Phi(z)}{dz^2} = \xi^{-2}\Phi(z) - \frac{\overline{T}\rho_q^{(1)2}(z)}{2\bar{\rho}_{ion}}, \tag{24}$$

and

$$e\psi(z) = -\frac{k_B T}{\bar{\rho}_{ion}}\left(\rho_q(z) - \rho_q^{(1)}(z)\Phi^{(1)}(z)\right). \tag{25}$$

The shapes of $\Phi(z)$ obtained from (24) in a semiinfinite system and in a slit are discussed in Sections IIIA and IIIB respectively.

A. OP profiles near a single wall

In the semiinfinite system the well-known solutions of (22) and (20) are

$$\rho_q^{(1)}(z) = -\kappa\sigma_0 e^{-\kappa z}, \tag{26}$$

and

$$\Phi^{(1)}(z) = \frac{h_0}{1+\xi^{-1}}e^{-z/\xi}. \tag{27}$$

We insert (26) in eqn (24), and from the boundary condition (18) we obtain

$$\Phi(z) = \frac{H_0}{1+\xi^{-1}}e^{-z/\xi} - B{\sigma_0}^2 e^{-2\kappa z}, \tag{28}$$

where

$$H_0 = h_0 + (1 + 2\kappa)B{\sigma_0}^2, \tag{29}$$

and

$$B = \frac{\overline{T}y^2}{2\bar{\rho}_{ion}(4y^2-1)} \approx \frac{3y^2}{\bar{\rho}_{ion}(4y^2-1)}. \tag{30}$$

The last equality in (30) is valid for $\bar{T} \approx \bar{T}_c$. Eqn (28)–(30) are valid for $z \gtrsim \xi, 1/\kappa$, due to the assumptions made in derivation of the coarse-grained description.

Note that the effect of the charges on the OP profile is twofold. First, the surface field h_0 is renormalized, and the renormalized H_0 depends on h_0 and on σ_0, $\bar{\rho}_{ion}$, κ and ξ. The surface field has a microscopic range, and the first contribution to the excess OP $\Phi(z)$ is a result of the critical correlations. The additional term in eqn (28) has the same decay length as the "external field", $\rho_q^{(1)2}(z)$.

For $y < 1/2$ the asymptotic decay of $\Phi(z)$ at large z is determined by the second term in (28). In such a case $\Phi(z) > 0$ for large z for both hydrophilic and hydrophobic surfaces, since $-B > 0$ for $y < 1/2$. Moreover, this term depends only on σ_0. This is because for $\xi < z < 1/2\kappa$ the effect of the surface selectivity is negligible, but near the wall there is an excess number density of ions, and ions are soluble in water.

For $y > 1/2$ the first term in (28) determines the behavior at large z. In the case of hydrophilic surfaces (with $h_0 > 0$) $|H_0| > |h_0|$. In the case of hydrophobic surfaces either $|H_0| < |h_0|$, or the effective surface field changes sign, $H_0 > 0$. The prefactor H_0 can be positive in the case of a hydrophobic surface when the surface charge is large, because $B > 0$ for $y > 1/2$.

In order to understand the physical reason for changing the weakly hydrophobic surface into effectively hydrophilic one, recall that the charged surface attracts oppositely charged ions. As a result of the entropy of mixing, excess of the number

density of ions near the surface is also present. The excess of water-soluble ions acts as an external field for the OP (see the last term in the integrand in eqn (14)). This 'external field' enhances the effect of the surface field h_0 in the case of the hydrophilic surface, and competes with h_0 in the case of the hydrophobic surface. If the 'external field' is much stronger than the selectivity of the surface due to the short-range wall–fluid interactions, then excess of water can occur near the hydrophobic surface. We discuss in more detail in what conditions $\Phi(z)$ is nonmonotonic in Appendix B.

Note that $B \to \infty$ for $y \to 1/2$. However, for $y = 1/2$ the decay rates of the two terms in (28) are the same, and the singularities in (28) cancel against each other. Assuming $\xi, z \gg 1$ and $\bar{T} \approx \bar{T}_c = 6$ we obtain for $y = 1/2$

$$\Phi(z) = h_0\left[1 + \alpha_0\frac{z}{\xi}\right]e^{-z/\xi}, \tag{31}$$

where $\alpha_0 = \dfrac{3{\sigma_0}^2}{8\bar{\rho}_{ion}h_0}$. When $\alpha_0 > 1$ or $\alpha_0 < 0$ then the profile (31) is nonmonotonic. Characteristic OP profiles near the hydrophilic and the hydrophobic surface are shown in Fig. 2.

The nonmonotonic OP profile has been obtained previously in charge-neutral critical systems in the case of weak surface fields[14,15,17,32] as a result of correlations between critical fluctuations. In our case the RHS in eqn (17) can be negative when the "external field" $\rho_q(z)^2$ is sufficiently large compared to $\Phi(z)$. As a result, a maximum of $\Phi(z)$ can be present when h_0 is small compared to σ_0, in some analogy to the weak surface fields in neutral systems. Note that the surface field is 'strong' or 'weak' in comparison with the surface charge.

B. OP profiles in a slit

In the slit the solution of the linearized EL equation for the charge distribution is (see (21), (6), (7))

$$\rho_q^{(1)}(z) = \frac{-\kappa}{S}\left[S_0e^{-\kappa z} + S_Le^{-\kappa(L-z)}\right]. \tag{32}$$

The coefficients in eqn (32) and the explicit expression for the solution of eqn (25) and (6) with the Neumann BC (7) for $\rho_q(z)$ are given in Appendix C.

The solution $\Phi^{(1)}(z)$ of the linearized EL eqn (20) with the BC (18) has the form

$$\Phi^{(1)}(z) = n_0e^{-z/\xi} + n_Le^{-(L-z)/\xi}, \tag{33}$$

with the coefficients given in Appendix D. Finally, the solution of eqn (24) with $\rho_q^{(1)}(z)$ given in eqn (32), and with the boundary conditions (18) is

$$\Phi(z) = A_0(L)e^{-z/\xi} + A_L(L)e^{-(L-z)/\xi} - {S_0}^2Q(L)e^{-2\kappa z} - {S_L}^2Q(L)e^{-2\kappa(L-z)} + S_0S_LCe^{-\kappa L}, \tag{34}$$

with the coefficients given in Appendix D. In Fig. 3 we show the profiles in a slit with identical hydrophilic surfaces for fixed temperature and surface properties, for weak (left plot) and strong (right plot) surface charge and for different widths of the

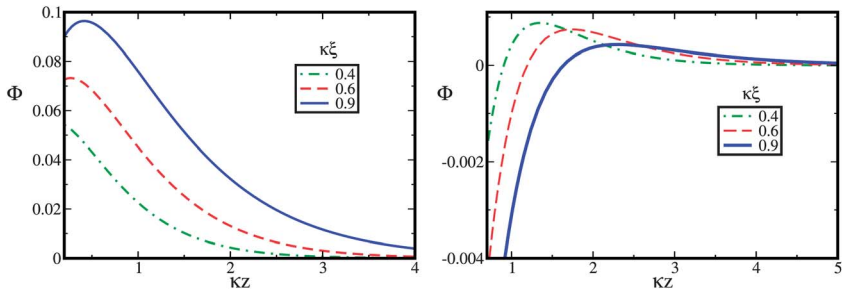

Fig. 2 The OP (excess concentration) in the semiinfinite system defined in eqn (10) and approximated by eqn (28). The dimensionless number density of ions, the inverse screening length and the surface field are $\bar{\rho}_{ion} = 10^{-3}$, $\kappa = 0.1$ and $|h_0| = 0.05$ respectively (the length unit is the molecular size a). (Left) The wall is hydrophilic and the charge density is $\sigma_0 = 0.016$. (Right) The wall is hydrophobic and the charge density is $\sigma_0 = 0.007$.

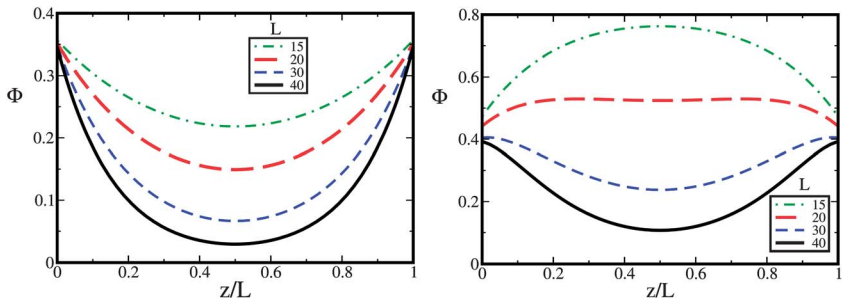

Fig. 3 The OP (excess concentration) in a slit defined in eqn (10) and approximated by eqn (34). The identical walls are hydrophilic. The dimensionless surface field, the number density of ions, the inverse screening length and the correlation length are $h_0 = 0.4$, $\bar{\rho}_{ion} = 10^{-3}$, $\kappa = 0.1$ and $\xi = 6$, respectively. (Left) Weak surface charge, $\sigma_0 = 0.006$. (Right) Strong surface charge, $\sigma_0 = 0.025$. From the top to the bottom line the width of the slit is $L = 15$, 20, 30, and 40. The length unit is the molecular size a.

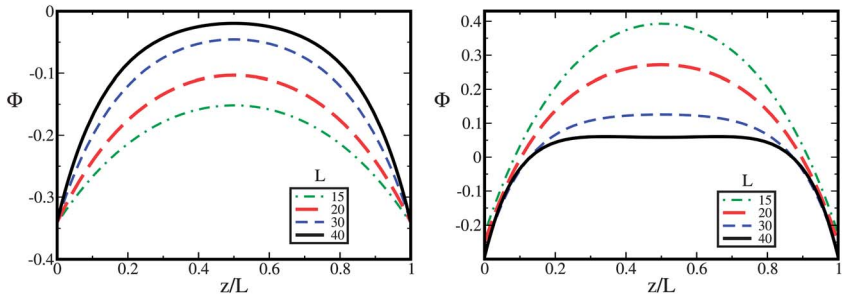

Fig. 4 The OP (excess concentration) in a slit defined in eqn (10) and approximated by eqn (34). The identical walls are hydrophobic. The dimensionless surface field, the number density of ions, the inverse screening length and the correlation length are $h_0 = -0.4$, $\bar{\rho}_{\text{ion}} = 10^{-3}$, $\kappa = 0.1$ and $\xi = 6$ respectively. (Left) Weak surface charge, $\sigma_0 = 0.006$. From the bottom to the top line the width of the slit is $L = 15, 20, 30, 40$. (Right) Strong surface charge, $\sigma_0 = 0.025$. From the top to the bottom line the width of the slit is $L = 15, 20, 30, 40$. The length unit is the molecular size a.

slit. In Fig. 4 analogous profiles are shown for identical hydrophobic surfaces.

In Fig. 5 we show the concentration profiles for the strongly selective and weakly charged left surface, and the weakly selective and strongly charged right surface. The strongly charged weakly selective surface (either hydrophilic or hydrophobic) acts as an effectively hydrophilic one because of the relatively high concentration of inorganic ions near the surface, and the preferential solubility of the ions in water (see the cartoon in Fig. 6). As we show in the next subsection, this fact can lead to a different sign of the Casimir potential than predicted by eqn (1).

We can summarize that the charged hydrophilic surface acts as even more hydrophilic, whereas the charged hydrophobic surface becomes less hydrophobic, and can lead even to excess of water if the surface charge is large and ions are soluble in water.

IV. The effective potential

We have shown that the presence of hydrophilic ions near the selective surfaces can lead to significant qualitative modifications

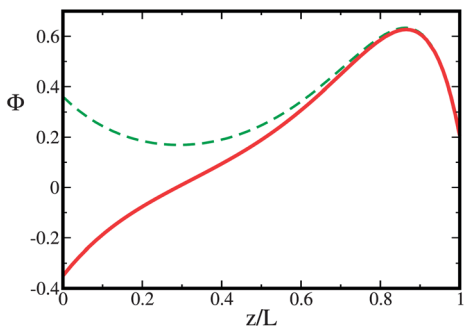

Fig. 5 The OP (excess concentration) in a slit defined in eqn (10) and approximated by eqn (34). One surface is strongly selective and weakly charged, whereas the other surface is weakly selective and strongly charged. The dimensionless surface fields, surface charge densities, the number density of ions, the inverse screening length, the correlation length and the width of the slit are $|h_0| = 0.4$, $|h_L| = 0.001$, $\sigma_0 = 0.001$, $\sigma_L = 0.05$, $\bar{\rho}_{\text{ion}} = 10^{-3}$, $\kappa = 0.1$, $\xi = 8$ and $L = 30$ (the length unit is the molecular size a). The left wall is hydrophobic (solid line), or hydrophilic (dashed line). The curves for weakly hydrophilic or weakly hydrophobic right wall are almost the same, and are indistinguishable on the plot.

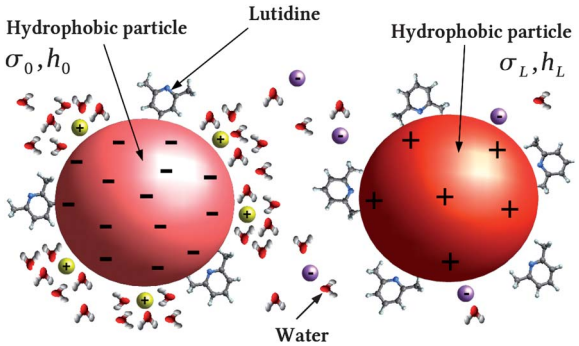

Fig. 6 Schematic representation of the distribution of the components in the case of colloid particles. Repulsion can appear between surfaces with opposite charges and like selectivity when $\sigma_0 \gg \sigma_L$ and $h_0 \ll h_L$ and the Debye length is bigger than the correlation length. The theory has been developed for a slit geometry. The distribution of the components and the interaction between curved surfaces of the colloid particles, however, have the same qualitative features and can be obtained by using the Derjaguin approximation.[27]

of the concentration profile in the slit (Fig. 3–5). In this section we determine the effect of these modifications of the OP on the effective interactions between the surfaces. In the approximation consistent with (24) the excess grand potential takes the form

$$\beta\mathscr{L} \approx \int_0^L \mathrm{d}z \left[\frac{\overline{\beta}}{2}\left(\xi^{-2}\Phi^2 + (\nabla\Phi)^2\right) - \frac{\rho_{\text{q}}^{(1)2}\Phi}{2\bar{\rho}_{\text{ion}}}\right] + \beta\mathscr{L}_{\text{C}}^{\text{s}} + \beta\mathscr{L}_{\text{DH}}[\rho_{\text{q}}] \tag{35}$$

where $\beta\mathscr{L}_{\text{C}}^{\text{s}}$ and $\beta\mathscr{L}_{\text{DH}}[\rho_{\text{q}}]$ are given in eqn (15) and (16). In thermodynamic equilibrium $\rho_{\text{q}}^{(1)}$, Φ, ρ_{q} and ψ satisfy eqn (22), (24), (25) and (6) respectively. Using the above equations and the BC (7) and (18), integrating by parts and approximating $\rho_{\text{q}}^{(1)2}\Phi$ by $\rho_{\text{q}}^{(1)2}\Phi^{(1)}$ we obtain

$$\beta\mathscr{L} \approx \frac{1}{4\bar{\rho}_{\text{ion}}}\int_0^L \mathrm{d}z\rho_{\text{q}}^{(1)2}(z)\Phi^{(1)}(z) + \frac{\beta}{2}\left(\sigma_0\psi(0) + \sigma_L\psi(L)\right) - \frac{\overline{\beta}}{2}\left(h_0\Phi(0) + h_L\Phi(L)\right). \tag{36}$$

In the critical region and for weak ionic strength ξ, $1/\kappa \gg 1$, so we can make the approximations $1 + \xi^{-1} \approx 1$, $1 + \kappa \approx 1$. We

use (32), (34) and Appendix C, subtract the surface tension contributions, assume the MF result $\bar{\beta} \approx 1/6$ for the near-critical temperature, and finally obtain the explicit asymptotic expression for the effective interactions (per microscopic area a^2) for $y < 1$,

$$\beta\Psi(L) \approx -\frac{A_\xi}{\xi}\mathrm{e}^{-L/\xi} + \frac{\kappa A_\kappa}{\bar{\rho}_{\mathrm{ion}}}\mathrm{e}^{-\kappa L} + \frac{\kappa A_{2\kappa}}{\bar{\rho}_{\mathrm{ion}}}\mathrm{e}^{-2\kappa L} \tag{37}$$

where the terms that decay faster are neglected,

$$A_\xi = \frac{2h_0h_L}{\overline{T}} + \frac{y^2\left({\sigma_0}^2h_L + {\sigma_L}^2h_0\right)}{\bar{\rho}_{\mathrm{ion}}(4y^2-1)} \tag{38}$$

and

$$A_\kappa = 2\sigma_0\sigma_L - \frac{2y(1+y)\sigma_0\sigma_L(h_0+h_L)}{(2y+1)}. \tag{39}$$

The above two amplitudes agree precisely with the corresponding amplitudes obtained in ref. 27 (note the different definitions of the surface fields here and in ref. 27). For $y < 1$, however, $\mathrm{e}^{-2\kappa L} > \mathrm{e}^{-L/\xi}\mathrm{e}^{-\kappa L}$, and instead of the term $\propto \mathrm{e}^{-L/\xi}\mathrm{e}^{-\kappa L}$ taken into account in ref. 27 for $y > 1$, we include in (37) the term $\propto \mathrm{e}^{-2\kappa L}$. The corresponding amplitude is

$$A_{2\kappa} = \left[\left({\sigma_0}^2 + {\sigma_L}^2\right) - \left({\sigma_0}^2h_0 + {\sigma_L}^2h_L\right)\left(\frac{2y(y+1)}{2y+1}\right) - \left({\sigma_0}^2h_L + {\sigma_L}^2h_0\right)\left(\frac{y(4y^2-2)}{4y^2-1}\right)\right]. \tag{40}$$

For $y < 1$ it is necessary to include the last term in eqn (37) in order to correctly describe the distances $L \simeq 1/2\kappa$ even on the level of the linearized EL equations. In the DH theory for non-adsorbing surfaces ($h_0 = h_L = 0$) the amplitude simplifies to $A_{2\kappa} = {\sigma_0}^2 + {\sigma_L}^2$.

The first term in (38) is the MF Casimir amplitude, and the first terms in (39) and (40) are the amplitudes in the effective electrostatic potential between the surfaces in the DH theory. The effective potential can be approximated by (1) supplemented with the term $\frac{\kappa({\sigma_0}^2 + {\sigma_L}^2)}{\bar{\rho}_{\mathrm{ion}}}\exp(-2\kappa L)$ when the correction terms in (38)–(40) are negligible. However, the correction and the leading-order terms in A_ξ are comparable if either ${\sigma_0}^2/\bar{\rho}_{\mathrm{ion}}$ is comparable with h_0, or ${\sigma_L}^2/\bar{\rho}_{\mathrm{ion}}$ is comparable with h_L. Recall that in such a case the OP profile (28) is non-monotonic near the respective wall (see Appendix B). Thus, we can expect significant deviation from the MF Casimir amplitude when the surface charges lead to a qualitative change of $\Phi(z)$. This is analogous to the nonuniversal Casimir potential in the case of weak surface fields leading to a nonmonotonic OP profile in charge-neutral systems.[15,17]

The amplitude $|A_\kappa|$ that governs the large-distance decay of $\beta\psi(L)$ (see (39)) is smaller for hydrophilic surfaces (h_0, $h_L > 0$) than for hydrophobic surfaces (h_0, $h_L < 0$). Thus the screening of the hydrophilic surface by hydrophilic ions is better than the screening of the hydrophobic surface. In addition, from (38) we can see that A_ξ is larger for hydrophilic surfaces than for hydrophobic surfaces. This is because the presence of hydrophilic ions enhances the hydrophilicity of the hydrophilic surface, and competes with the hydrophobicity of the hydrophobic surface. Thus, the hydrophilic ions lead to opposite changes of the effective potential for hydrophilic and hydrophobic surfaces.

Terms of higher order in the surface charges and the surface fields are neglected in (38)–(40). For large differences between the fields some of the neglected terms can be relevant, therefore for different orders of magnitude of σ_0, σ_L and h_0, h_L our results can deviate from the exact solution on a quantitative level. We discuss this issue in Section V.

The correction terms in both A_ξ and $A_{2\kappa}$ diverge for $y = 1/2$. However, for $y = 1/2$ the decay rates ξ and $1/2\kappa$ are the same, and the divergent terms cancel against each other. For $y = 1/2$ we obtain from (37)

$$\beta\Psi(L) \approx \frac{\kappa A_\kappa}{\bar{\rho}_{\mathrm{ion}}}\,\mathrm{e}^{-\kappa L} + \frac{\kappa B_{2\kappa}(L)}{\bar{\rho}_{\mathrm{ion}}}\,\mathrm{e}^{-2\kappa L} \tag{41}$$

with finite coefficients given in Appendix E.

A. Identical surfaces

Let us discuss in more detail the case of two identical surfaces, $h_0 = h_L$, $\sigma_0 = \sigma_L$, relevant for interactions between identical colloidal particles. In the special case of $y = 1/2$ and $h_0 = h_L$, $\sigma_0 = \sigma_L$ the amplitudes in eqn (41) are

$$A_\kappa = {\sigma_0}^2\left(2 - \frac{3}{2}h_0\right) \tag{42}$$

and

$$B_{2\kappa}(L) = 2{\sigma_0}^2 - \frac{4\bar{\rho}_{\mathrm{ion}}{h_0}^2}{\overline{T}} - \frac{h_0{\sigma_0}^2}{2}(3 + 2\kappa L). \tag{43}$$

$A_\kappa > 0$ for weak surface fields to which analytical expressions are restricted. Thus, the repulsion dominates at large distances.

At shorter distances, the form of $\Psi(L)$ depends on the sign and magnitude of $B_{2\kappa}(L)$. The Casimir attraction competes with the electrostatic repulsion in the first two terms in (43). The correction term in (43) is negative for hydrophilic and positive for hydrophobic surfaces. From (43) it follows that the surface charge must be smaller for hydrophobic than for hydrophilic surfaces to overcome the electrostatic repulsion and obtain attraction at short distances. Similar behavior is found for $y \neq 1/2$, as shown in Fig. 7. In the lowest-order approximation (1) the effective potential is the same between two hydrophobic surfaces and between two hydrophilic surfaces if the surface charges and the absolute values of the surface fields are the same. The coupling between the concentration and the charge distributions can lead to qualitative differences of the effective interactions between two hydrophobic or two hydrophilic surfaces with the same values of σ_0 and $|h_0|$.

In Fig. 8 we demonstrate the sensitivity of $\Psi(L)$ to the surface charge. For weak surface charge (left panel) we can see a crossover from the SALR type potential (attraction at short and repulsion at large distances) for $\xi = 4$ (green dashed-dotted line) to the attractive potential for $\xi = 9$ (solid blue line). For stronger surface charge (right panel), the potential far away from T_c is

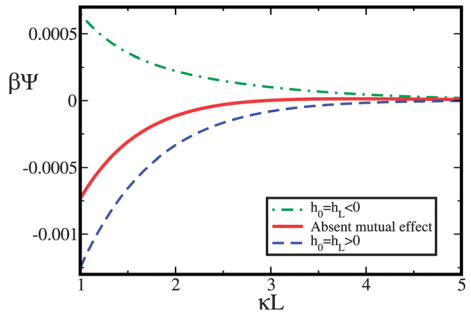

Fig. 7 The effective potential per microscopic area in k_BT/a^2 units, eqn (41), for the dimensionless surface charge $\sigma_0 = \sigma_L = 0.004$, the number density of ions $\bar{\rho}_{ion} = 0.001$ and the dimensionless surface field $|h_0| = |h_L| = 0.4$. The inverse Debye length is $\kappa = 0.1$ and the correlation length is $\xi = 8$; length is in units of the microscopic size a. The effect of the charge distribution on the critical adsorption is neglected for the solid line. Dashed and dash-dotted lines represent the hydrophilic and hydrophobic surfaces, respectively.

repulsive at large separations, and assumes a maximum for smaller separation between the surfaces. On approaching T_c the maximum changes to a minimum.

B. Significant deviations from eqn (1)

Here we focus on the question for which surface properties the effective potential can deviate significantly from eqn (1). The electrostatic repulsion is proportional to $\sigma_0\sigma_L$, and is weak when the surface charge at one surface is small. The MF Casimir amplitude is proportional to h_0h_L, and is weak when one of the surface fields is small. We thus need to find such surface charges and surface fields for which one of the correction terms in (38) and (39) is larger than both $\sigma_0\sigma_L/\bar{\rho}_{ion}$ and h_0h_L. This is possible when the strongly selective surface is weakly charged, and the weakly selective one is strongly charged ($\sigma_L \gg \sigma_0$ and $h_L \ll h_0$). In such a case the term $\sigma_L{}^2h_0/\bar{\rho}_{ion}$ can dominate.

We focus on $y = 1/2$ where the analysis is simpler. When $\sigma_0h_L \ll \sigma_L$ and $\sigma_0{}^2 \ll h_0$, then the term with the largest amplitude is (see Appendix E)

$$\beta\Psi(L) \simeq -\frac{\sigma_L{}^2h_0}{2}\kappa L e^{-2\kappa L}. \quad (44)$$

Attraction and repulsion is expected for $h_0 > 0$ and $h_0 < 0$ respectively. The potential (37) is shown in Fig. 9 (left) and Fig. 9 (right) for like and opposite surface charges respectively. The corresponding OP profiles are shown in Fig. 5.

Note that when both the Casimir and the electrostatic potentials are *repulsive*, *attraction* at intermediate distances, followed by a small repulsion barrier, occurs when one surface is strongly hydrophilic and weakly charged, and the other one is weakly hydrophobic and strongly charged. Such a phenomenon was observed experimentally between a colloid particle and a substrate in ref. 6. When the Casimir and the DH potential are *both attractive*, the potential between two oppositely charged hydrophobic surfaces can be *repulsive* at intermediate distances, and very weakly attractive at larger distances (see the cartoon in Fig. 6). This may happen when one of the two

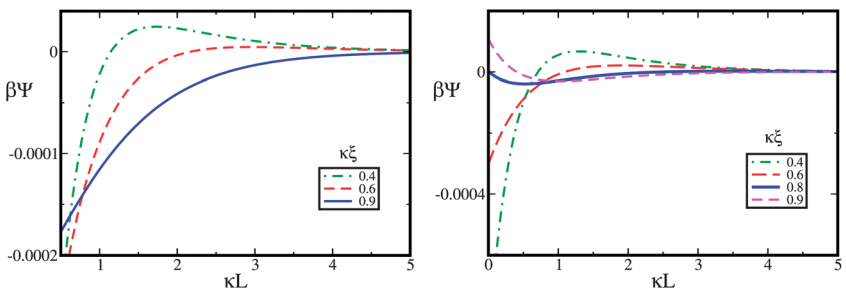

Fig. 8 The effective potential per microscopic area in k_BT/a^2 units, eqn (41), between identical hydrophobic walls with $h_0 = -0.14$, $\kappa = 0.1$, and the dimensionless number density of ions $\bar{\rho}_{ion} = 0.001$. (Left) $\sigma_0 = 0.001$. (Right) $\sigma_0 = 0.0013$.

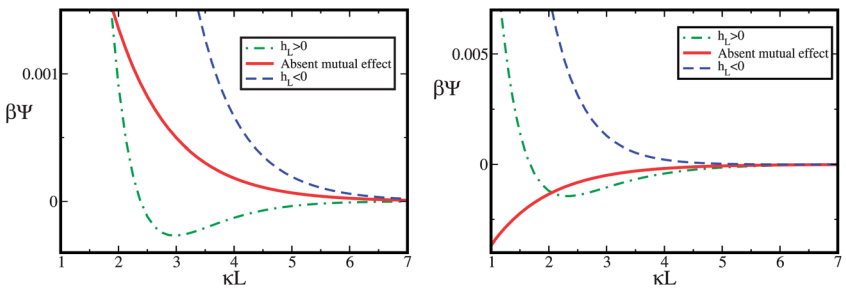

Fig. 9 The effective potential $\beta\Psi(L)$ per microscopic area in k_BT/a^2 units, given by eqn (1) (central curves) and by eqn (37) (top and bottom curves) for strong selectivity and small surface charge at one surface and weak selectivity and large surface charge at the other surface. The dimensionless density of ions is $\bar{\rho}_{ion} = 0.001$, the correlation length is $\xi = 8$ and the inverse screening length is $\kappa = 0.1$. The length unit is the molecular size a. (Left) $\sigma_0 = 0.05$ and $\sigma_L = 0.001$ and (right) $\sigma_0 = 0.05$ and $\sigma_L = -0.001$, and the dimensionless surface fields are $h_L = 0.4$ and $h_0 = \pm 0.001$ (central and bottom curves), and $h_L = -0.4$, $h_0 = \pm 0.001$ (top curves). The curves with $h_0 = 0.001$ and $h_0 = -0.001$ cannot be distinguished on the plot.

surfaces is strongly hydrophobic and weakly charged, and the other one is weakly hydrophobic and strongly charged. In such a case the second surface behaves as a hydrophilic one (see Fig. 5 and 9), and in the case of weak electrostatic attraction the Casimir repulsion can dominate.

When the surface charge and selectivity of the two confining surfaces are both much different, then the total potential can be qualitatively different than in eqn (1). Attraction can be present when both terms in (1) are repulsive, and repulsion can be present when both terms in (1) are attractive. The strongly hydrophilic and hydrophobic surfaces show *opposite* trends. The strongly hydrophilic surface always leads to more attractive, and the strongly hydrophobic one always leads to more repulsive potential if the surfaces are charged.

V. Comparison of the approximate analytical expressions with numerical solutions of the full EL equations

The main result of this work, eqn (37)–(40), was obtained under numerous assumptions and approximations. We assumed that the system is near the critical point and the concentration of ions is small, so that the correlation and the screening lengths are both much larger than the molecular size. Next we assumed that the dimensionless surface charges and surface fields are comparable and small. This assumption allows to truncate the expansion of the entropy in terms of ρ_q and Φ at the lowest-order nontrivial term. However, for very large differences between the surface charges and the surface fields, as well as very close to the critical point where $\xi^{-2} \to 0$, the neglected contributions to the entropy become relevant. In this case the approximate expression may deviate from the exact result obtained by the solutions of the full EL eqn (6) and (50)–(52).

In this subsection we check the validity of eqn (37)–(40) for various conditions. We solve numerically eqn (6) and (52)–(54) with the help of the package "bvpSolve". bvpSolve numerically solves boundary value problems (BVP) of ordinary differential equations (ODE). There are three methods for solving ODE in this package. For our purpose we choose "bvptwp" which is a mono-implicit Runge–Kutta (MIRK) method with deferred corrections by using conditioning in the mesh selection. In addition, we solve numerically eqn (6), (17) and (19). In the latter case we consider the approximate functional (14), but do not make further approximations for its EL equations. In Fig. 10 and 11 we plot the numerical and the approximate analytical results for the OP profile (34) and for the effective potential (37) respectively for comparable surface charges and surface fields. As expected, good quantitative agreement is obtained when all the assumptions made in derivations of the approximate expressions are satisfied (Fig. 11).

For significant differences between the surface charges and the surface fields the approximate expressions deviate from the numerical results, as shown in Fig. 12, and only semi-quantitative agreement is obtained. Nevertheless, we are convinced that the essential physics behind the strong mutual effects of the ions and critical adsorption, especially attraction when both

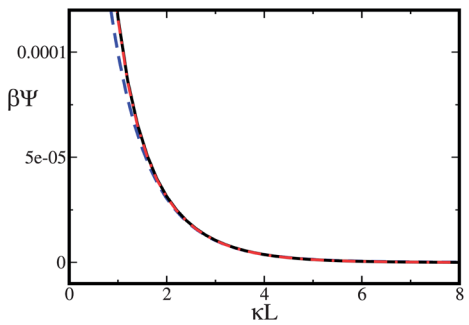

Fig. 11 The effective potential per microscopic area, $\beta\Psi/a^2$, where a is the molecular size. The dimensionless surface fields are $h_0 = h_L = 0.006$ and the dimensionless surface charge density is $\sigma_0 = \sigma_L = 0.001$. The dimensionless density of ions is $\bar{\rho}_{ion} = 0.001$, the inverse screening length is $\kappa = 0.1$ and $y = 0.645$. The length unit is the molecular size a. The dashed line is eqn (37), the dash-dotted line is numerical solution to the approximate EL equations (eqn (6), (17) and (19)), and the solid line is the numerical solution to the full EL equations (eqn (6) and (50)–(52)).

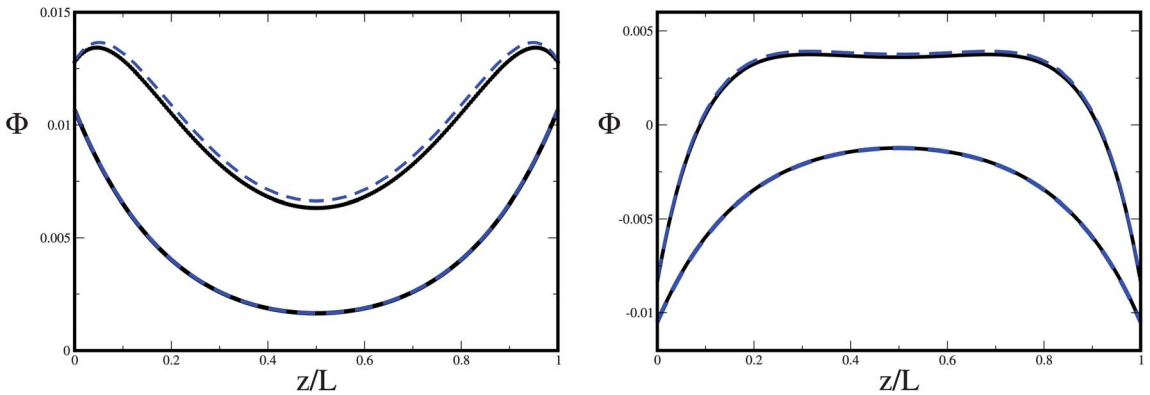

Fig. 10 The OP profiles for (Left) hydrophilic surfaces and (Right) hydrophobic surfaces with the dimensionless surface fields $h_0 = h_L = \pm 0.012$ and dimensionless surface charge density $\sigma_0 = \sigma_L = 0.005$ (top curves), and $\sigma_0 = \sigma_L = 0.001$ (bottom curves). The dimensionless density of ions is $\bar{\rho}_{ion} = 0.001$, the inverse screening length is $\kappa = 0.1$ and $y = 0.745$. The length unit is the molecular size a. Dashed-lines represent eqn (34) and solid lines represent numerical solutions of the full EL equations.

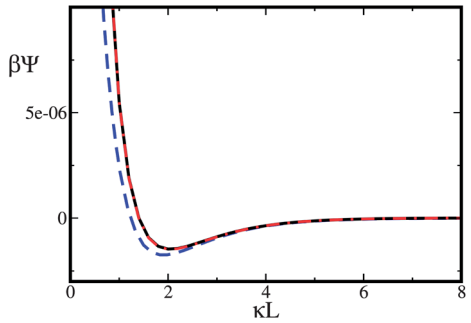

Fig. 12 The effective potential per elementary area, $\beta\Psi/a^2$, where a is the molecular size. The dimensionless surface fields are $h_0 = -0.04$, $h_L = -0.01$ and the dimensionless surface charge density is $\sigma_0 = 0.001$ and $\sigma_L = -0.0001$. The dimensionless density of ions is $\bar{\rho}_{\text{ion}} = 0.001$, the inverse screening length is $\kappa = 0.1$ and $y = 0.645$. The length unit is the molecular size a. The dashed line is eqn (37), the dash-dotted line is numerical solution to the approximate EL equations (eqn (6), (17) and (19)), and the solid line is the numerical solution to the full EL equations (eqn (6) and (50)–(52)).

terms in (1) are repulsive and repulsion when both terms in (1) are attractive, is captured by our formulae (37)–(40).

VI. Summary

We have developed a new version of the Landau-type functional for confined near-critical binary mixture with ions. The new functional (see eqn (14)–(16)) depends only on two fields – the charge density $\rho_q(z)$ and the concentration difference between inorganic and organic components, $\Phi(z)$. In standard experiments the inorganic components are water and dissociating salt such as KBr. By minimizing the functional we obtained Euler–Lagrange equations, and next considered their approximate version (see (24) and (25)) that can be solved analytically. Unlike in ref. 27, we focused on the case where the Debye screening length is larger than the correlation length of critical fluctuations.

By considering first a semiinfinite system we have found that the key factor that determines the shape of Φ is the parameter $\sigma_0^2/(\bar{\rho}_{\text{ion}}|h_0|)$, where σ_0 is the surface charge, $\bar{\rho}_{\text{ion}}$ is the bulk density of ions, and $|h_0|$ is the surface selectivity. If this parameter is large, then $\Phi(z)$ can be nonmonotonic, and near the weakly hydrophobic surface excess of water can occur. Thus, in the critical region the charged hydrophobic surface can behave as an *effectively hydrophilic* one. The reason for this behavior is the large amount of hydrophilic ions near the strongly charged surface. Preferential solubility of the ions in water dominates in this case over the weak hydrophobicity of the surface. Let us discuss the physics behind this behavior in more detail. Near the hydrophobic surface an excess of oil in a layer of thickness $\sim\xi$ is predicted by the theory of critical adsorption.[8–11] If this surface is charged, then the excess number density of ions in a layer of the thickness $1/2\kappa$ is predicted by the Debye–Hückel theory.[18] However, because of much lower solubility of the ions in oil than in water, a simultaneous excess of oil and of ions in a thick layer near the surface is associated with a large internal-energy penalty. The distribution of the ions as well as the solvent composition near the surface must be a compromise between the bulk tendency to separate the ions from the oil, and the surface preference to attract both immiscible components.

In the case of a slit with identical surfaces the shape of $\Phi(z)$ can be qualitatively different from the concentration profile for charge-neutral surfaces. In particular, excess of water can occur in the center of the slit with hydrophobic surfaces. These strong effects of the charges again occur when the ratio between $\sigma_0^2/\bar{\rho}_{\text{ion}}$ and $|h_0|$ is large.

We have obtained the approximate analytical expression for the effective potential (see (37)–(40)). The two dominant terms decay as in eqn (1), but with amplitudes depending on y. The amplitudes are the same as found previously for the correlation length larger than the screening length. The correction term decays as $\propto \exp(-2\kappa L)$.

We have found that when the charged surface with stronger selectivity is hydrophilic, the potential is more attractive, and when it is hydrophobic, the potential is more repulsive than predicted by (1). When the two identical confining surfaces are hydrophilic, then attraction between them can occur even when repulsion is expected from eqn (1). When the two identical confining surfaces are hydrophobic, then repulsion between them can occur even when attraction is expected from eqn (1).

The most spectacular violation of (1) is found when one surface is weakly hydrophobic and strongly charged, and the other surface is weakly charged and strongly selective. The origin of the violation of (1) is the effectively hydrophilic nature of the strongly charged and weakly hydrophobic surface. If the second surface is strongly hydrophilic and weakly charged, we obtain attraction, although both terms in (1) are repulsive. Such unexpected behavior was observed experimentally in ref. 6. If the second surface is weakly charged with opposite sign and it is strongly hydrophobic, we obtain repulsion, although both terms in (1) are attractive. Future experiments should verify this prediction.

Our findings can have numerous applications. In addition to the macro-phase separation,[7] a microphase separation can be induced by very small temperature changes when the maximum in the potential is present (see Fig. 8). Not only one-type of particles, as in ref. 7, but also mixtures of oppositely charged colloidal particles, which form ordered structures resembling ionic crystals in noncritical solvents[33] can undergo reversible phase transitions. We are convinced that there can be many more applications of the control over the effective interactions. Our expressions can help to design the experimental studies.

VIII. Appendix A: EL equations and approximate Landau-type functional

We consider the functional (3) in terms of the new variables (eqn (8), (10) and (11)), and with u_{vdw} given in eqn (9). In the case of close packing

$$\sum_{i=1}^{4}\frac{\mu_i\rho_i}{J} = \mu_0^* + \mu_\Phi^*\Phi + \mu_{\text{ion}}^*\rho_{\text{ion}} \tag{45}$$

where $\mu_0^* = \frac{\mu_w + \mu_+}{2J}$, $\mu_\Phi^* = \frac{\mu_w - \mu_l}{2J}$ and $\mu_{\text{ion}}^* = \frac{\mu_+ - \mu_w}{J}$. The entropy is given by

$$-\frac{Ts}{J} = \overline{T}\int_0^L \mathrm{d}z\left(\frac{1-2\rho_{\text{ion}}(z)+\Phi(z)}{2}\right)\ln\left(\frac{1-2\rho_{\text{ion}}(z)+\Phi(z)}{2}\right) + \left(\frac{1-\Phi(z)}{2}\right)\ln\left(\frac{1-\Phi(z)}{2}\right) + \left(\frac{\rho_{\text{ion}}(z)+\rho_{\text{q}}(z)}{2}\right)\ln\left(\frac{\rho_{\text{ion}}(z)+\rho_{\text{q}}(z)}{2}\right) + \left(\frac{\rho_{\text{ion}}(z)-\rho_{\text{q}}(z)}{2}\right)\ln\left(\frac{\rho_{\text{ion}}(z)-\rho_{\text{q}}(z)}{2}\right). \tag{46}$$

In the bulk $\rho_{\text{q}} = 0$, and we restrict our attention to the critical composition $\bar{\Phi} = 0$. In thermodynamic equilibrium the number density of ions in the bulk, $\bar{\rho}_{\text{ion}} = \text{const.}$, satisfies the extremum condition for the grand potential, and from $\frac{\partial\omega}{\partial\overline{\rho}_{\text{ion}}} = 0$ we obtain

$$\mu_{\text{ion}}^* = \overline{T}\ln R \tag{47}$$

where

$$R = \frac{\overline{\rho}_{\text{ion}}}{1-2\overline{\rho}_{\text{ion}}}. \tag{48}$$

On the other hand, in the presence of the external surface we obtain from the extremum condition $\frac{\delta\omega}{\delta\rho_{\text{ion}}} = 0$

$$\mu_{\text{ion}}^* = \overline{T}\ln\left(\frac{\sqrt{{\rho_{\text{ion}}}^2(z) - {\rho_{\text{q}}}^2(z)}}{1-2\rho_{\text{ion}}(z)+\Phi(z)}\right). \tag{49}$$

By equating RHS of eqn (47) and (49) we obtain

$$\rho_{\text{ion}}(z) = \frac{-2R^2\big(1+\Phi(z)\big) + \sqrt{{\rho_{\text{q}}}^2(z)(1-4R^2) + R^2\big(1+\Phi(z)\big)^2}}{1-4R^2}. \tag{50}$$

With the help of eqn (50) we can eliminate $\rho_{\text{ion}}(z)$ from (46). The remaining EL equations are obtained in a similar way, and have the forms

$$e\beta\psi(z) + \frac{1}{2}\ln\left(\frac{\rho_{\text{ion}}(z)+\rho_{\text{q}}(z)}{\rho_{\text{ion}}(z)-\rho_{\text{q}}(z)}\right) = 0, \tag{51}$$

and

$$\frac{\mathrm{d}^2\Phi(z)}{\mathrm{d}z^2} = -6\Phi + \frac{\overline{T}}{2}\ln\left[\frac{1-2\rho_{\text{ion}}(z)+\Phi(z)}{\big(1-\Phi(z)\big)\big(1-2\rho_{\text{ion}}(z)\big)}\right]. \tag{52}$$

Eqn (50)–(52) and (6) form a closed set of two differential and two algebraic equations.

We introduce $\vartheta = \rho_{\text{ion}}(z) - \bar{\rho}_{\text{ion}}$, and assume that if the surface charge and the surface field are not large, then $|\Phi| \ll 1$, $|\rho_{\text{q}}| \ll 1$ and $|\vartheta| \ll 1$. Note that the internal energy is independent of ρ_{ion}. In order to calculate the excess grand potential associated with ϑ, we need to calculate the excess of entropy and the excess of (45). Expanding (46), taking into account (47) and the analogous equation for μ_Φ^*, and keeping only the lowest-order terms we obtain

$$-\frac{T}{J}\big(s[\rho_{\text{q}},\,\Phi,\,\rho_{\text{ion}}] - s[0,\,0,\,\bar{\rho}_{\text{ion}}]\big) - (\mu_\Phi\Phi + \mu_{\text{ion}}\vartheta) \approx \overline{T}\int_0^L \mathrm{d}z\left[\frac{1}{1-2\bar{\rho}_{\text{ion}}}\left(\frac{1-\bar{\rho}_{\text{ion}}}{2}\Phi^2(z) + \frac{1}{2\bar{\rho}_{\text{ion}}}\vartheta^2(z) - \Phi(z)\vartheta(z)\right) + \frac{{\rho_{\text{q}}}^2(z)}{2{\bar{\rho}_{\text{ion}}}^2}\big(\bar{\rho}_{\text{ion}} - \vartheta(z)\big)\right]. \tag{53}$$

Finally, by minimizing (53) with respect to the noncritical OP $\vartheta(z)$ we obtain eqn (14).

IX. Appendix B: nonmonotonic $\Phi(z)$ in a semiinfinite system

From eqn (28) we find that $\mathrm{d}\Phi(z)/\mathrm{d}z = 0$ for real positive z when the surface field and the surface charge satisfy the condition

$$\frac{\overline{\rho}_{\text{ion}}h_0}{3{\sigma_0}^2} < \frac{y^2}{2y+1} < \frac{1}{3} \tag{54}$$

where $\bar{T} \approx \bar{T}_{\text{c}}$ and $y < 1$. $\Phi(z)$ assumes the extremum for

$$z = \frac{\xi}{2y-1}\ln\left(\frac{2yB{\sigma_0}^2}{H_0}\right). \tag{55}$$

When $h_0 < 0$ the OP profile is nonmonotonic for $y < 1/2$, as discussed in Section 3a, and for $y > 1/2$ if $H_0 > 0$, or explicitly

$$\frac{\overline{\rho}_{\text{ion}}h_0}{3{\sigma_0}^2} > -\frac{(1+2\kappa)y^2}{4y^2-1} \tag{56}$$

X. Appendix C: the charge distribution

The coefficients in eqn (32) are

$$\begin{cases} S_0 = \sigma_0 + \sigma_L\mathrm{e}^{-\kappa L}, \\ S_L = \sigma_L + \sigma_0\mathrm{e}^{-\kappa L}, \\ S = 1 - \mathrm{e}^{-2\kappa L}. \end{cases} \tag{57}$$

The explicit form of the charge–density profile with the effect of the critical adsorption included is (see eqn (25), (6) and (7))

$$\rho_q(z) = \frac{\kappa}{S}\left[a_0 e^{-\kappa z} + a_L e^{-\kappa(L-z)} - S_0 n_0 g_1 e^{-\kappa z} e^{-z/\xi} - S_L n_L g_1 e^{-\kappa(L-z)} e^{-(L-z)/\xi} + S_0 n_L g_2 e^{-\kappa z} e^{-(L-z)/\xi} + S_L n_0 g_2 e^{-\kappa(L-z)} e^{-z/\xi}\right], \quad (58)$$

where

$$\begin{cases} a_0 = -S_0 + \frac{S_0 n_0}{S} g_3 + \frac{S_L}{S}[n_L g_3 - n_0 g_4] e^{-\kappa L}\left(1 - e^{-L/\xi}\right) + \frac{S_0 n_L}{S} g_4\left(e^{-L/\xi} - e^{-2\kappa L}\right), \\ a_L = -S_L + \frac{S_L n_L}{S} g_3 + \frac{S_0}{S}[n_0 g_3 - n_L g_4] e^{-\kappa L}\left(1 - e^{-L/\xi}\right) + \frac{S_L n_0}{S} g_4\left(e^{-L/\xi} - e^{-2\kappa L}\right), \end{cases} \quad (59)$$

$$\begin{cases} g_1 = \frac{(1+y)^2}{(1+2y)}, \\ g_2 = \frac{(1-y)^2}{(2y-1)}, \\ g_3 = \frac{y(y+1)}{1+2y}, \\ g_4 = \frac{y(1-y)}{(2y-1)}, \end{cases} \quad (60)$$

S_0, S_L and S are given in (57), whereas n_0 and n_L are given in eqn (61). (The correct expressions (32) and (58) differ from that given in ref. 27 by terms $O(e^{-2\kappa L})$, which are negligible in the case of $y \gg 1$ studied in ref. 27.)

XI. Appendix D: coefficients in eqn (34)

The parameters in eqn (33) and (34) are

$$\begin{cases} n_0 = \frac{1}{1+\xi^{-1}}\left[h_0 - h_L \frac{1-\xi^{-1}}{1+\xi^{-1}} e^{-L/\xi}\right] \simeq_{\xi\to\infty} \left[h_0 - h_L e^{-L/\xi}\right], \\ n_L = \frac{1}{1+\xi^{-1}}\left[h_L - h_0 \frac{1-\xi^{-1}}{1+\xi^{-1}} e^{-L/\xi}\right] \simeq_{\xi\to\infty} \left[h_L - h_0 e^{-L/\xi}\right]. \end{cases} \quad (61)$$

where B is defined in eqn (30),

$$Q(L) = \frac{B}{(1-e^{-2\kappa L})^2} \simeq B\left(1 + 2e^{-2\kappa L}\right), \quad (63)$$

and

$$C = \frac{\overline{T} y^2}{\overline{\rho}_{ion}} \approx \frac{6y^2}{\overline{\rho}_{ion}}. \quad (64)$$

The RHS in the above equation is valid for $\bar{T} \approx \bar{T}_c$, and we have used the MF result $\bar{T}_c = 6$.

XII. Appendix E: coefficients in eqn (41)

$$A_\kappa = \sigma_0 \sigma_L\left[2 - \frac{3}{4}(h_0 + h_L)\right] \quad (65)$$

$$B_{2\kappa}(L) = {\sigma_0}^2 + {\sigma_L}^2 - \frac{4\overline{\rho}_{ion} h_0 h_L}{\overline{T}} - \frac{3\left({\sigma_0}^2 h_0 + {\sigma_L}^2 h_L\right)}{4} - \frac{\left({\sigma_0}^2 h_L + {\sigma_L}^2 h_0\right)}{2}\kappa L \quad (66)$$

Acknowledgements

FP gratefully acknowledges A. Roostaei for his help in the numerical steps. The work of FP was realized within the International PhD Projects Programme of the Foundation for Polish Science, co-financed from European Regional Development Fund within Innovative Economy Operational Programme Grants for innovation. AC acknowledges partial financial support by the NCN grant 2012/05/B/ST3/03302.

$$\begin{aligned} A_0(L) &= \frac{1}{1+\xi^{-1}}\Big[(2(2\kappa+1)B - C)\sigma_0\sigma_L e^{-\kappa L} - \frac{\xi-1}{\xi+1}\left(h_L + B{\sigma_L}^2(2\kappa+1)\right)e^{-L/\xi} \\ &\quad + \left((2\kappa+1)B\left(2{\sigma_0}^2 + {\sigma_L}^2\right) - (2\kappa-1)B{\sigma_L}^2 - C\left({\sigma_0}^2 + {\sigma_L}^2\right)\right)e^{-2\kappa L} + \left(h_0 + (2\kappa+1)B{\sigma_0}^2\right)\Big], \\ A_L(L) &= \frac{1}{1+\xi^{-1}}\Big[(2(2\kappa+1)B - C)\sigma_0\sigma_L e^{-\kappa L} - \frac{\xi-1}{\xi+1}\left(h_0 + B{\sigma_0}^2(2\kappa+1)\right)e^{-L/\xi} \\ &\quad + \left((2\kappa+1)B\left(2{\sigma_L}^2 + {\sigma_0}^2\right) - (2\kappa-1)B{\sigma_0}^2 - C\left({\sigma_0}^2 + {\sigma_L}^2\right)\right)e^{-2\kappa L} + \left(h_L + (2\kappa+1)B{\sigma_L}^2\right)\Big], \end{aligned} \quad (62)$$

References

1 C. N. Likos, *Phys. Rep.*, 2001, **348**, 267.
2 L. Belloni, *J. Phys.: Condens. Matter*, 2000, **12**, R549.
3 C. Hertlein, L. Helden, A. Gambassi, S. Dietrich and C. Bechinger, *Nature*, 2008, **451**, 172.
4 A. Gambassi, A. Maciołek, C. Hertlein, U. Nellen, L. Helden, C. Bechinger and S. Dietrich, *Phys. Rev. E: Stat., Nonlinear, Soft Matter Phys.*, 2009, **80**, 061143.
5 D. Bonn, J. Otwinowski, S. Sacanna, H. Guo, G. Wegdam and P. Schall, *Phys. Rev. Lett.*, 2009, **103**, 156101.
6 U. Nellen, J. Dietrich, L. Helden, S. Chodankar, K. Nygard, J. F. van der Veen and C. Bechinger, *Soft Matter*, 2011, **7**, 5360.
7 V. D. Nguyen, S. Faber, Z. Hu, G. H. Wegdam and P. Schall, *Nat. Commun.*, 2013, **4**, 1584.
8 M. E. Fisher and P. G. de Gennes, *C. R. Seances Acad. Sci., Ser. B*, 1978, **287**, 207.
9 H. W. Diehl, *Field-theoretic Approach to Critical Behavior at Surfaces, vol. 10 of Phase Transitions and Critical Phenomena*, Academic Press, London, 1st edn, 1986, pp. 75–267.
10 M. Krech, *Casimir Effect In Critical Systems*, World Scientific, Singapore, 1994.
11 M. Krech, *J. Phys.: Condens. Matter*, 1999, **11**, R391.
12 B. S. Pradip, V. D. Nguyen, A. V. Limaye and P. Schall, *Adv. Mater.*, 2013, **25**, 14991503.
13 J. L. Barrat and J.-P. Hansen, *Basic Concepts for Simple and Complex Liquids*, Cambridge University Press, 2003.
14 O. Vasilyev, A. Maciołek and S. Dietrich, *Phys. Rev. E: Stat., Nonlinear, Soft Matter Phys.*, 2010, **84**, 041605.
15 A. Maciołek, A. Ciach and A. Drzewiński, *Phys. Rev. E: Stat. Phys., Plasmas, Fluids, Relat. Interdiscip. Top.*, 1999, **60**, 2887.
16 A. Ciach and U. Ritschel, *Nucl. Phys. B*, 1997, **489**, 653.
17 D. B. Abraham and A. Maciołek, *Phys. Rev. E: Stat., Nonlinear, Soft Matter Phys.*, 2010, **105**, 055701.
18 J. N. Israelachvili, *Intermolecular and Surface Forces*, Academic Press, Boston, 3rd edn, 2011.
19 A. Stradner, H. Sedgwick, F. Cardinaux, W. Poon, S. Egelhaaf and P. Schurtenberger, *Nature*, 2004, **432**, 492.
20 A. Imperio and L. Reatto, *J. Chem. Phys.*, 2006, **124**, 164712.
21 A. J. Archer, *Phys. Rev. E: Stat., Nonlinear, Soft Matter Phys.*, 2008, **78**, 031402.
22 A. de Candia, E. DelGado, A. Fierro, N. Sator, M. Tarzia and A. Coniglio, *Phys. Rev. E: Stat., Nonlinear, Soft Matter Phys.*, 2006, **74**, 010403(R).
23 A. Ciach, *Phys. Rev. E: Stat., Nonlinear, Soft Matter Phys.*, 2008, **78**, 061505.
24 A. Ciach and W. T. Góźdź, *Condens. Matter Phys.*, 2010, **13**, 23603.
25 A. Ciach and A. Maciołek, *Phys. Rev. E: Stat., Nonlinear, Soft Matter Phys.*, 2010, **81**, 041127.
26 F. Pousaneh and A. Ciach, *J. Phys.: Condens. Matter*, 2011, **23**, 412101.
27 F. Pousaneh, A. Ciach and A. Maciołek, *Soft Matter*, 2012, **8**, 7567.
28 M. Bier, A. Gambassi, M. Oettel and S. Dietrich, *Europhys. Lett.*, 2011, **95**, 60001.
29 M. Bier, A. Gambassi and S. Dietrich, *J. Chem. Phys.*, 2013, **137**, 034504.
30 S. Samin and Y. Tsori, *Europhys. Lett.*, 2011, **95**, 36002.
31 S. Samin and Y. Tsori, *J. Chem. Phys.*, 2012, **136**, 154908.
32 T. F. Mohry, A. Maciołek and S. Dietrich, *Phys. Rev. E: Stat., Nonlinear, Soft Matter Phys.*, 2010, **81**, 061117.
33 M. Leunissen, C. Christova, A.-P. Hynninen, C. Royal, A. Campbell, A. Imhof, M. Dijkstra, R. van Roji and A. van Blaaderen, *Nature*, 2005, **437**, 235.